International Journal of Nanomedicine

Dovepress
Taylor & Francis Group

Open Access Full Text Article

ORIGINAL RESEARCH

DNA Aptamer-Functionalized Fluorescent Silica Nanoparticles: A Robust Strategy for Specific Detection and Bioimaging of HER2-Overexpressing Breast Cancer

Juntao Tan[1,*], Zixi Hu[2,*], Da Huang[1,*], Suqing Cheng[3,*], Lu Chen[1], Liangliang Min[1], Jianhong Tu[3], Zhihua Li[1,4]

[1]Jiangxi Province Key Laboratory of Breast Diseases, Nanchang People's Hospital, Nanchang People's Hospital Affiliated of Nanchang Medical College, Nanchang, Jiangxi, People's Republic of China; [2]Clinical Laboratory Center, The First affiliated hospital of Guilin Medical University, Guilin, Guangxi Zhuang Autonomous Region, People's Republic of China; [3]Department of Pathology, Nanchang People's Hospital, Nanchang People's Hospital Affiliated of Nanchang Medical College, Nanchang, Jiangxi, People's Republic of China; [4]Department of Breast Surgery, Nanchang People's Hospital, Nanchang People's Hospital Affiliated of Nanchang Medical College, Nanchang, Jiangxi, People's Republic of China

*These authors contributed equally to this work

Correspondence: Zhihua Li, Jiangxi Province Key Laboratory of Breast Diseases, Nanchang People's Hospital, Nanchang People's Hospital Affiliated of Nanchang Medical College, No. 2, Xiangshan South Road, Xihu District, Nanchang, Jiangxi, 330008, People's Republic of China, Tel/Fax +86 791 86617472, Email 13392605973@163.com; Jianhong Tu, Department of Pathology, Nanchang People's Hospital, Nanchang People's Hospital Affiliated of Nanchang Medical College, No. 2, Xiangshan South Road, Xihu District, Nanchang, Jiangxi, 330008, People's Republic of China, Tel/Fax +86 791 86617472, Email 18979464846@163.com

Background: Precise detection of HER2-positive breast cancer is vital for targeted therapy. This study integrates HER2-specific DNA aptamers with fluorescent silica nanoparticles (FSNPs) to develop a targeted imaging probe.

Methods: HER2 aptamer-conjugated FSNPs (HApt-FSNPs) were synthesized and characterized. Specificity was evaluated in HER2-positive/negative cells and tumor sections via flow cytometry and microscopy. Targeting efficacy and biodistribution were assessed in tumor-bearing mice through systemic injection and real-time fluorescence imaging. Photostability and biosafety were systematically examined.

Results: HApt-FSNPs showed uniform size, excellent dispersity, and enhanced photostability. They selectively bound HER2-positive cells and tumor tissues, with binding effectively blocked by free aptamer. In vivo imaging revealed specific accumulation in HER2-positive tumors, peaking at 6 hours post-injection, with minimal off-target signals. The probe demonstrated good biocompatibility in vitro and in vivo.

Conclusion: The HApt-FSNP platform enables specific detection and in vivo imaging of HER2-positive breast cancer, highlighting its potential for diagnostic and bioimaging applications.

Keywords: HER2-positive breast cancer, aptamer, fluorescent silica nanoparticles, in vivo imaging, targeted detection

Introduction

Breast cancer remains the most frequently diagnosed malignancy among women worldwide and exhibits substantial molecular heterogeneity, with HER2-positive breast cancer representing a distinct, aggressive subtype associated with poor prognosis and rapid progression if not treated promptly and accurately.[1–3] Accurate identification of HER2-positive tumor cells is therefore critical for clinical diagnosis, and molecular subtyping to guide treatment decisions, directly impacting therapeutic outcomes.[4,5] Specifically, determining HER2 status is a prerequisite for selecting appropriate HER2-targeted therapies, forming a cornerstone of precision medicine in breast cancer management. Currently, clinical HER2 status is routinely assessed by immunohistochemistry (IHC) or fluorescence in situ hybridization (FISH), which,

https://doi.org/10.2147/IJN.S591943
Received: 15 January 2026
Accepted: 27 February 2026
Published: 9 March 2026

despite clinical utility, rely on invasive biopsies and centralized laboratory processing,[6] limiting their applicability for real-time, high-throughput monitoring and early detection.

In recent years, nanotechnology-based detection strategies have emerged as promising alternatives, offering enhanced sensitivity, signal amplification capability, and adaptability to diverse biomedical scenarios, particularly for cancer biomarker sensing and imaging.[7–9]Nanoparticle-based probes have been shown to improve detection thresholds and enable functional imaging that complements conventional pathology.[10–12]

Aptamers are short single-stranded nucleic acids selected through Systematic Evolution of Ligands by Exponential Enrichment (SELEX) that can bind target molecules with high affinity and specificity through unique three-dimensional conformations.[13,14] Compared with antibodies, aptamers offer several advantages including low immunogenicity, high chemical stability, ease of modification, and reproducible chemical synthesis, making them attractive ligands for targeted cancer detection and biosensing.[15] Recent studies have successfully incorporated aptamers into nanomaterial-based probes for sensitive detection of HER2 and other tumor-associated biomarkers.[14,16,17]

Fluorescent silica nanoparticles (FSNPs) represent an ideal nanoplatform for bioimaging applications owing to their tunable size, excellent photostability, high brightness, chemical inertness, and facile surface modification.[18,19] Encapsulation of fluorophores within a silica matrix protects against photobleaching and enables signal amplification far beyond that of free dyes or single-fluorophore conjugates[20,21] Integration of aptamer-mediated targeting with FSNP-based signal enhancement presents a robust strategy for developing sensitive and specific detection systems for cancer biomarkers such as HER2.

In this study, we constructed HER2 aptamer-conjugated FSNPs (HApt-FSNPs) for the highly specific detection and imaging of HER2-positive breast cancer. The nanoparticles were comprehensively characterized, and their targeting specificity, photostability, cytocompatibility, and biosafety were systematically evaluated across cellular, tissue, and in vivo models. We propose that this platform functions as a pre-therapeutic diagnostic tool for molecular subtyping. By enabling non-invasive or minimally invasive identification of HER2 status, it could provide critical information to guide the subsequent selection of HER2-targeted therapies, thereby contributing to the advancement of precision medicine. Our findings establish HApt-FSNPs as a promising targeted fluorescent probe with potential for both ex vivo diagnostic applications and non-invasive in vivo imaging.

Materials and Methods

Materials

All chemical reagents, including tetraethyl orthosilicate (TEOS), ammonia solution (25–28%), absolute ethanol, (3-aminopropyl)triethoxysilane (APTES), N-hydroxysuccinimide (NHS), 1-ethyl-3-(3-dimethylaminopropyl)carbodiimide (EDC), fluorescein isothiocyanate (FITC), and Cyanine5.5 NHS ester (Cy5.5-NHS), were of analytical grade and purchased from Sigma Chemical (St. Louis, USA). Ultrapure water (Milli-Q, 18.2 MΩ·cm) was used throughout the experiments.

Design, Synthesis, and Characterization of Oligonucleotides

The HER2-specific DNA aptamer (HApt) and a scrambled control aptamer (Scr) were designed and synthesized by a commercial provider (eg, Sangon Biotech, Shanghai, China) with high-performance liquid chromatography (HPLC) purification. The complete nucleotide sequence of HApt is 5′-AACCGCCCAAATCCCTAAGAGTCTGCACTTGTCATTTTGTATATGTATTTGGTTTTTGGCTCTCACAGACACACTACACACGCACA-3′. This sequence is identical to the core HER2-binding sequence reported in a previous study.[22] For in vitro experiments, the HApt was synthesized with a 5′-FITC label and carried a 3′-terminal amine ($-NH_2$) modification for subsequent conjugation. For in vivo imaging, the same core sequence was synthesized with a 5′-Cy5.5 label and a 3′-NH_2 group. The scrambled control aptamer (Scr; 5′-AAAAAAAAAAAAAAACGTGCAGTACGCCAACCTTTCTCATGCGCTGCCCCTCTTA-3′) was synthesized with a 3′-NH_2 group; its randomized sequence has no known affinity for HER2. All oligonucleotide sequences, modifications, and the reported dissociation constant (Kd ≈ 18.9 nM) for HApt are summarized in Supplementary Table S1. Prior to use, lyophilized

aptamers were reconstituted in nuclease-free water, heated at 95 °C for 5 min, and then gradually cooled to room temperature to facilitate proper folding into their active secondary structures.

Synthesis of Fluorescent FSNPs

Fluorescent silica nanoparticles were prepared via a modified Stöber sol-gel process.[23] For particles intended for in vitro studies, FITC was first conjugated to APTES according to a published protocol to obtain FITC-APTES, which was then co-condensed with TEOS in an ethanol-water-ammonia mixture. For in vivo applications, Cy5.5-NHS was similarly conjugated to APTES to form Cy5.5-APTES prior to silica network formation. In a typical synthesis, 2 mL of TEOS and 0.2 mL of the respective dye-functionalized silane were added dropwise to a mixture containing 40 mL ethanol, 10 mL water, and 2 mL ammonia solution under vigorous stirring at room temperature. The reaction proceeded for 12 h, after which the resulting FSNPs were collected by centrifugation (12,000 rpm, 15 min), washed repeatedly with ethanol and water, and finally redispersed in ultrapure water.

Surface Functionalization and Aptamer Conjugation

Carboxyl groups were introduced onto the FSNP surface by incubating the particles with succinic anhydride in dimethyl sulfoxide for 4 h at room temperature. The carboxylated FSNPs were then activated using EDC/NHS chemistry in MES buffer (pH 6.0) for 30 min. The amine-modified aptamers (HApt or Scr) were added at a molar ratio of approximately 200:1 (aptamer: estimated nanoparticle number) and allowed to react overnight at 4 °C with gentle shaking. Unconjugated aptamers were removed by three cycles of centrifugation (12,000 rpm, 15 min) and washing with PBS (pH 7.4). The final HApt-FSNPs and Scr-FSNPs were resuspended in PBS and stored at 4 °C in the dark. The average number of aptamers per nanoparticle was estimated by comparing the decrease in supernatant absorbance at 260 nm before and after conjugation, yielding an approximate density of 160 ± 15 aptamers per particle.

Physicochemical Characterization

Hydrodynamic size distribution and polydispersity index (PDI) of FSNPs and HApt-FSNPs were measured by dynamic light scattering (DLS) at room temperature. Zeta potential was determined to assess surface charge changes after aptamer conjugation. Nanoparticle morphology and size were examined using transmission electron microscopy (TEM). Fourier-transform infrared (FT-IR) spectroscopy was employed to analyze surface chemical composition and confirm aptamer modification. UV–Vis absorption spectra and fluorescence emission spectra were recorded to evaluate optical properties.

Cell Culture

The HER2-positive breast cancer cell lines SKBR3 and BT-474, HER2-negative breast cancer cell lines MCF-7 and MDA-MB-231, and normal cell lines HEK293T and L-02 were purchased from the Cell Bank of the Chinese Academy of Sciences (Shanghai, China). All cell lines were cultured in complete medium supplemented with fetal bovine serum and antibiotics. The cells were maintained at 37°C in a humidified atmosphere with 5% CO_2.

Flow Cytometry Analysis of Cellular Binding

Cells were harvested and incubated with HApt-FSNPs, Scr-FSNPs, or bare FSNPs for a fixed incubation period at 37 °C. After incubation, cells were washed thoroughly to remove unbound nanoparticles and resuspended in buffer for flow cytometry analysis. Fluorescence signals were recorded, and binding efficiency was quantified using median fluorescence intensity (MFI). All experiments were performed in three independent biological replicates (n = 3).

Fluorescence Microscopy Imaging

Cells were seeded on coverslips and incubated with the indicated nanoparticle formulations. After washing, nuclei were counterstained, and cells were fixed. Fluorescence images were acquired using a [Nikon Ti2] microscope with a 20× objective, using fixed exposure times (200 ms for FITC channel) and gain settings across all compared samples. Quantitative analysis of fluorescence intensity per field was performed using image analysis software and normalized as indicated.

Competitive Blocking Assay

To confirm aptamer-mediated specificity, HER2-positive SKBR3 cells were pre-incubated with an excess amount of free HApt prior to treatment with HApt-FSNPs. Binding efficiency was subsequently evaluated by flow cytometry and fluorescence microscopy.

Photostability Assessment

HApt-FSNPs and free FITC-labeled HApt were subjected to continuous illumination under fluorescence microscopy. Images were acquired at 0, 1, 5, and 10 min. Fluorescence intensity was quantified and normalized to the initial signal to assess photobleaching behavior.

In vitro Cytocompatibility Evaluation

The cytocompatibility of HApt-FSNPs was evaluated using a CCK-8 assay. HEK293T and L-02 cells were incubated with HApt-FSNPs at concentrations of 0.1, 0.5, and 1.0 mg/mL for 12, 24, and 48 h, respectively. Cell viability was calculated relative to untreated control cells.

In vivo Biosafety Evaluation

Healthy SPF BALB/c mice (female, 4–6 weeks old, 18–22 g) were randomly divided into two groups and intravenously administered HApt-FSNPs or PBS as control. Mice were monitored daily for general condition and body-weight changes. After 7 days, mice were anesthetized with inhalational isoflurane in oxygen (2–3% induction, 1–2% maintenance). Euthanasia was performed by CO_2 inhalation using a gradual-fill method (10–30% chamber volume/min), followed by cervical dislocation as a secondary confirmatory method. Major organs (heart, lung, liver, spleen, and kidney) were collected, fixed, paraffin-embedded, sectioned, and stained with hematoxylin and eosin (H&E) for histological examination.

Tumor Tissue Section Staining

HER2-positive (SKBR3) and HER2-negative (MCF-7) tumor tissues were harvested from xenografted tumor-bearing BALB/c nude mice (female, 4–6 weeks old). Mice were anesthetized with inhalational isoflurane in oxygen (2–3% induction, 1–2% maintenance), and euthanasia was performed by CO_2 inhalation (gradual-fill, 10–30% chamber volume/min) followed by cervical dislocation prior to tumor collection. Fresh tumor tissues were snap-frozen in optimal cutting temperature (OCT) compound and cryosectioned into 5 μm thick slices. After fixation with 4% paraformaldehyde for 15 minutes, sections were washed with PBS and permeabilized with 0.1% Triton X-100 for 10 minutes. Non-specific binding was blocked using 5% BSA for 1 hour at room temperature. The tumor tissue sections were then incubated with 100 μg/mL HApt-FSNPs for 1 hour at 37 °C. As specificity controls, sections were treated with bare FSNPs, Scr-FSNPs, or HApt-FSNPs with competitive blocking using excess free HApt. After washing, the sections were stained with DAPI to visualize the cell nuclei. Fluorescence microscopy was performed to assess HApt-FSNP binding to HER2-positive and HER2-negative tumor sections. Fluorescence intensity was quantified using ImageJ software.

In vivo Fluorescence Imaging and Biodistribution Studies

To assess the in vivo targeting and biodistribution profile of HApt-FSNPs, fluorescence imaging studies were performed in tumor-bearing mouse models. HApt-FSNPs were administered via tail vein injection to mice bearing subcutaneous HER2-positive (SKBR3) and HER2-negative (MCF-7) xenografts. For direct comparison of targeting specificity, both tumor models were included in the study.

Real-time whole-body fluorescence imaging was conducted at predetermined time points (0.5, 2, 6, 12, and 24 hours post-injection) using a small animal in vivo imaging system. The system was configured to detect the emission wavelength of the encapsulated fluorophore (Cy5.5), enabling longitudinal monitoring of nanoparticle distribution and tumor accumulation. Regions of interest (ROIs) were defined over the tumor sites and major organ regions, and fluorescence intensity was quantified to evaluate the kinetics of tumor targeting and systemic clearance.

At the terminal time point (24 hours), mice were euthanized, and major organs (heart, lungs, liver, spleen, kidneys) along with tumors were excised for ex vivo imaging. The fluorescence signals of harvested tissues were captured under identical imaging conditions to determine the final biodistribution of HApt-FSNPs. Quantitative analysis of fluorescence intensity was performed using ImageJ software, comparing signals between HER2-positive and HER2-negative tumors, as well as across different organs, to assess targeting specificity and organ uptake. Each experimental group consisted of 5 mice (n =5).

Statistical Analysis

Data are expressed as mean ± standard deviation (SD). All statistical analyses were performed using GraphPad Prism 9.0. For flow-cytometry and fluorescence quantification experiments, comparisons between two groups were analyzed using two-tailed Student's *t*-test, while comparisons among more than two groups were assessed by one-way ANOVA with Tukey's multiple comparisons test. Cell viability assays were analyzed based on normalized absorbance values relative to untreated controls. Photostability data were analyzed by repeated measurements over time and compared using one-way ANOVA at individual time points. A P value < 0.05 was considered statistically significant (*P < 0.05, **P < 0.01, ***P < 0.001)

Ethics Statement

All animal experiments were approved by the Institutional Animal Care and Use Committee of Guilin Medical University (approval No. GLMU202517013) and conducted in accordance with institutional guidelines, the Guide for the Care and Use of Laboratory Animals, and the AVMA Guidelines for the Euthanasia of Animals.[24] Mice were maintained under SPF conditions, and efforts were made to minimize pain and distress. For procedures requiring anesthesia, mice were anesthetized with inhalational isoflurane in oxygen (2–3% induction, 1–2% maintenance) with anesthetic depth confirmed by loss of pedal withdrawal reflex. Euthanasia was performed by CO_2 inhalation using a gradual-fill method (10–30% chamber volume/min), followed by cervical dislocation as a secondary confirmatory method; death was verified prior to tissue collection.

Results

Schematic Illustration of HApt-FSNP Design and Detection Strategy

Figure 1 schematically illustrates the design and application of HApt-FSNPs for the selective detection of HER2-positive breast cancer cells. The HER2-specific DNA aptamer is conjugated onto the surface of FSNPs, enabling specific recognition of HER2-overexpressing cells. The encapsulated fluorescent dyes within the silica matrix provide enhanced fluorescence stability, forming the basis for sensitive and reliable cellular detection.

Physicochemical Characterization of HApt-FSNPs

The physicochemical properties of FSNPs before and after aptamer functionalization were systematically characterized (Figure 2 and Supplementary Table S2). DLS analysis showed that bare FSNPs possessed a uniform hydrodynamic diameter of 78.9 ± 4.7 nm with a narrow PDI of 0.131 ± 0.025, indicating good colloidal stability. After conjugation with HApt, the average hydrodynamic diameter increased to 86.6 ± 5.3 nm, accompanied by a slightly reduced PDI (0.113 ± 0.017), consistent with the formation of an aptamer layer on the nanoparticle surface without inducing aggregation.

TEM further confirmed that both FSNPs and HApt-FSNPs exhibited uniform spherical morphology with smooth surfaces and well-defined nanoscale structures (Figure 2A and B). Importantly, aptamer functionalization did not alter the overall morphology or integrity of the silica nanoparticles.

Zeta-potential measurements revealed a clear surface charge shift following aptamer conjugation. Bare FSNPs displayed a negative zeta potential of −32.9 ± 2.9 mV, characteristic of silica surfaces, whereas HApt-FSNPs exhibited a more negative potential (−38.3 ± 3.2 mV), reflecting the contribution of the negatively charged phosphate backbone of the DNA aptamer (Figure 2C).

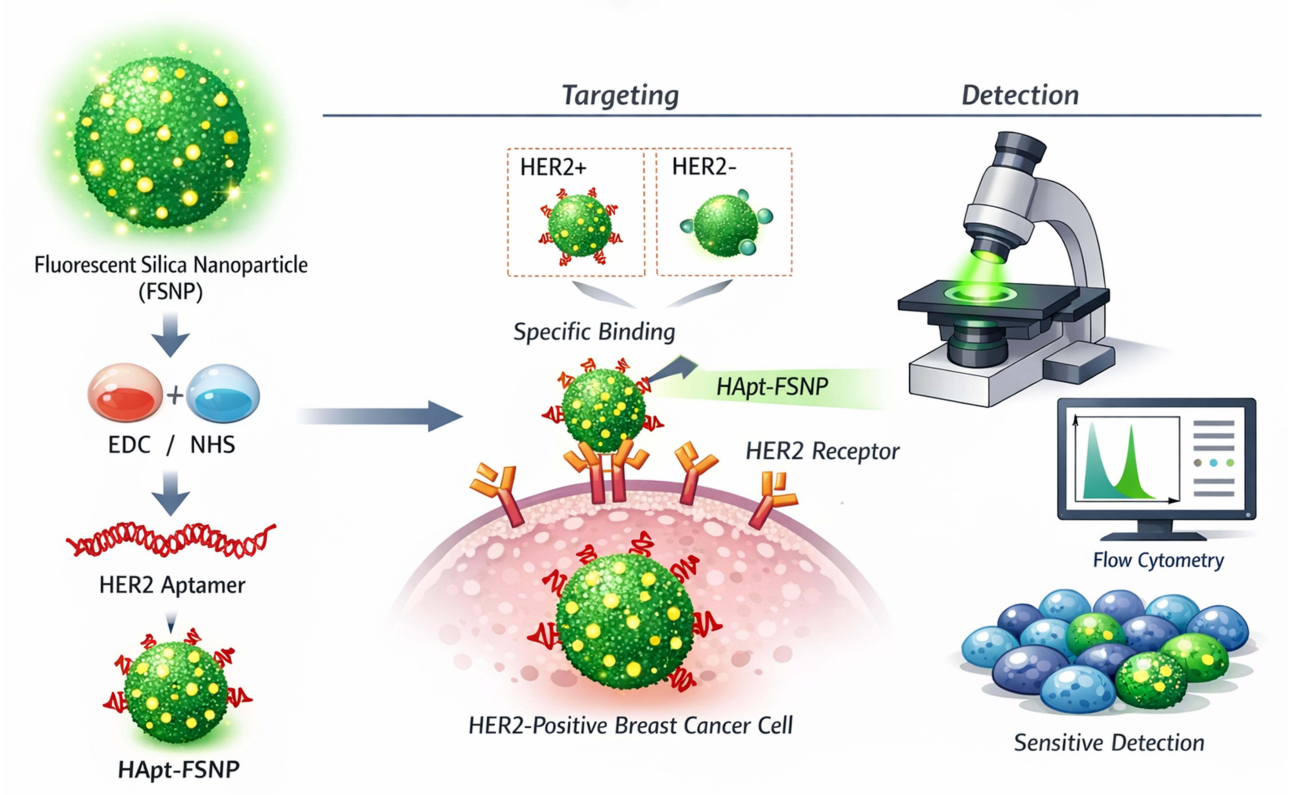

Figure 1 Schematic illustration of HApt functionalized FSNPs for highly specific detection of HER2-positive breast cancer.

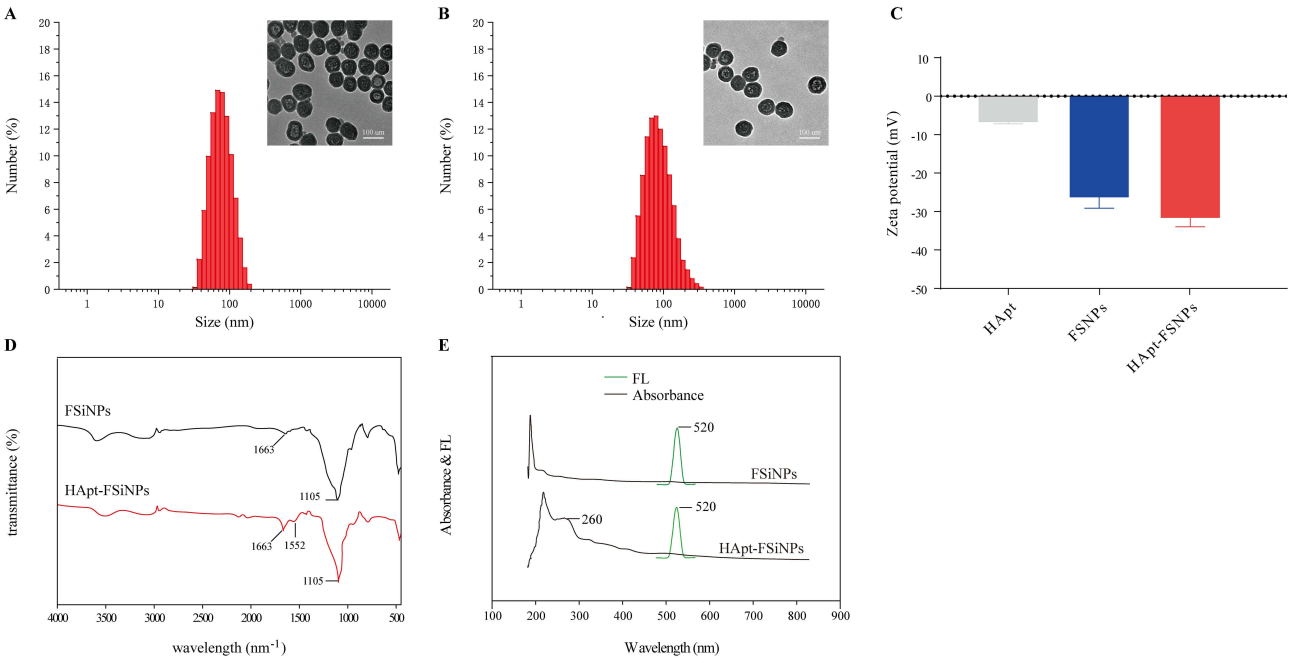

Figure 2 Characterization of HApt-FSNPs. (**A**) Size distribution and TEM image (inset) of FSNPs. (**B**) Size distribution and TEM image (inset) of HApt-FSNPs. Scale bar = 100 nm. (**C**) Zeta potential of aptamer HApt, FSNPs and HApt-FSNPs. (**D**) FT-IR spectra of FSNPs (black line) and HApt-FSNPs (red line). (**E**) UV–Vis absorbance (red line) and fluorescence emission spectra (black dotted line) of FSNPs and HApt-FSNPs.

https://doi.org/10.2147/IJN.S591943

FT-IR spectroscopy provided direct evidence for successful chemical conjugation of HApt to the FSNP surface (Figure 2D). In addition to the characteristic Si–O–Si stretching vibration observed at approximately 1105 cm^{-1}, HApt-FSNPs displayed new absorption bands at 1663 cm^{-1}, corresponding to C=O stretching vibrations of amide bonds, and at 1552 cm^{-1}, attributed to amide II vibrations arising from C–N stretching and N–H bending. These features confirm covalent attachment of the amine-modified aptamer onto carboxyl-functionalized FSNPs.

The optical properties of FSNPs and HApt-FSNPs were further evaluated by UV–Vis absorption and fluorescence emission spectroscopy (Figure 2E). HApt-FSNPs exhibited a distinct absorption peak at 260 nm, characteristic of nucleic acids and absent in bare FSNPs, indicating successful aptamer conjugation. Both FSNPs and HApt-FSNPs showed a prominent fluorescence emission peak centered at approximately 520 nm, corresponding to the encapsulated fluorescent dye, with no significant shift or intensity loss after aptamer modification. These results demonstrate that surface functionalization preserved the intrinsic fluorescence properties of the nanoparticles.

Validation of HER2 Expression in Cell Lines

To independently confirm the HER2 expression profile of the cellular models used in this study, flow cytometry was performed using a fluorescently labeled anti-HER2 antibody. As shown in Supplementary Figure 1, the HER2-positive cell lines SKBR3 and BT-474 displayed markedly elevated mean fluorescence intensity (MFI). In contrast, the HER2-negative lines MCF-7 and MDA-MB-231 showed only background-level fluorescence, consistent with their well-established phenotypes. This direct validation confirms the appropriateness of these cell lines for assessing the HER2-targeting specificity of our nanoprobe.

Specific Recognition of HER2-Positive Breast Cancer Cells

The targeting capability of HApt-FSNPs toward HER2-positive breast cancer cells was evaluated using flow cytometry and fluorescence microscopy (Figure 3). Flow-cytometry analysis revealed strong fluorescence signals in HER2-positive SKBR3 and BT-474 cells following incubation with HApt-FSNPs, whereas HER2-negative MCF-7 and MDA-MB-231 cells exhibited minimal fluorescence (Figure 3A). Quantitative analysis of MFI further confirmed significantly higher binding of HApt-FSNPs to HER2-positive cells compared with HER2-negative controls (Figure 3B).

Consistent with these findings, fluorescence microscopy demonstrated intense green fluorescence localized on the surface of HER2-positive cells treated with HApt-FSNPs, while negligible fluorescence was observed in HER2-negative cells under identical conditions (Figure 3C). Quantification of fluorescence intensity per field showed a marked enhancement in HER2-positive cells, with signals normalized to SKBR3 cells (Figure 3D). These results collectively demonstrate the high specificity of HApt-FSNPs for HER2-overexpressing breast cancer cells.

Specificity Validation and Competitive Blocking Assay

To further verify aptamer-mediated specificity, control and competitive blocking experiments were performed in HER2-positive SKBR3 cells (Figure 4). Flow-cytometry histogram overlays demonstrated that bare FSNPs and Scr-FSNPs exhibited weak fluorescence signals, indicating minimal nonspecific binding, whereas HApt-FSNPs produced a pronounced rightward shift in fluorescence intensity (Figure 4A). Notably, pre-incubation with excess free HApt (blocking group) markedly attenuated the fluorescence signal of HApt-FSNPs, suggesting effective competitive inhibition. Quantitative analysis of the flow-cytometry data further confirmed these observations. As shown in Figure 4B, the MFI of HApt-FSNPs was significantly higher than that of FSNPs and Scr-FSNPs, while the blocking group exhibited a pronounced reduction in MFI compared with the HApt-FSNP group (***$P < 0.001$), although remaining slightly higher than background levels.

Consistent results were obtained from fluorescence microscopy analysis. Representative images showed strong membrane-associated fluorescence in SKBR3 cells treated with HApt-FSNPs, whereas minimal fluorescence was observed in the FSNP, Scr-FSNP, and blocking groups (Figure 4C). Quantitative analysis of fluorescence intensity per field confirmed a significant decrease in normalized fluorescence intensity in the blocking group relative to the HApt-FSNP group (Figure 4D). Collectively, these results demonstrate that the cellular binding of HApt-FSNPs is predominantly mediated by specific HApt–HER2 interactions rather than nonspecific nanoparticle adsorption.

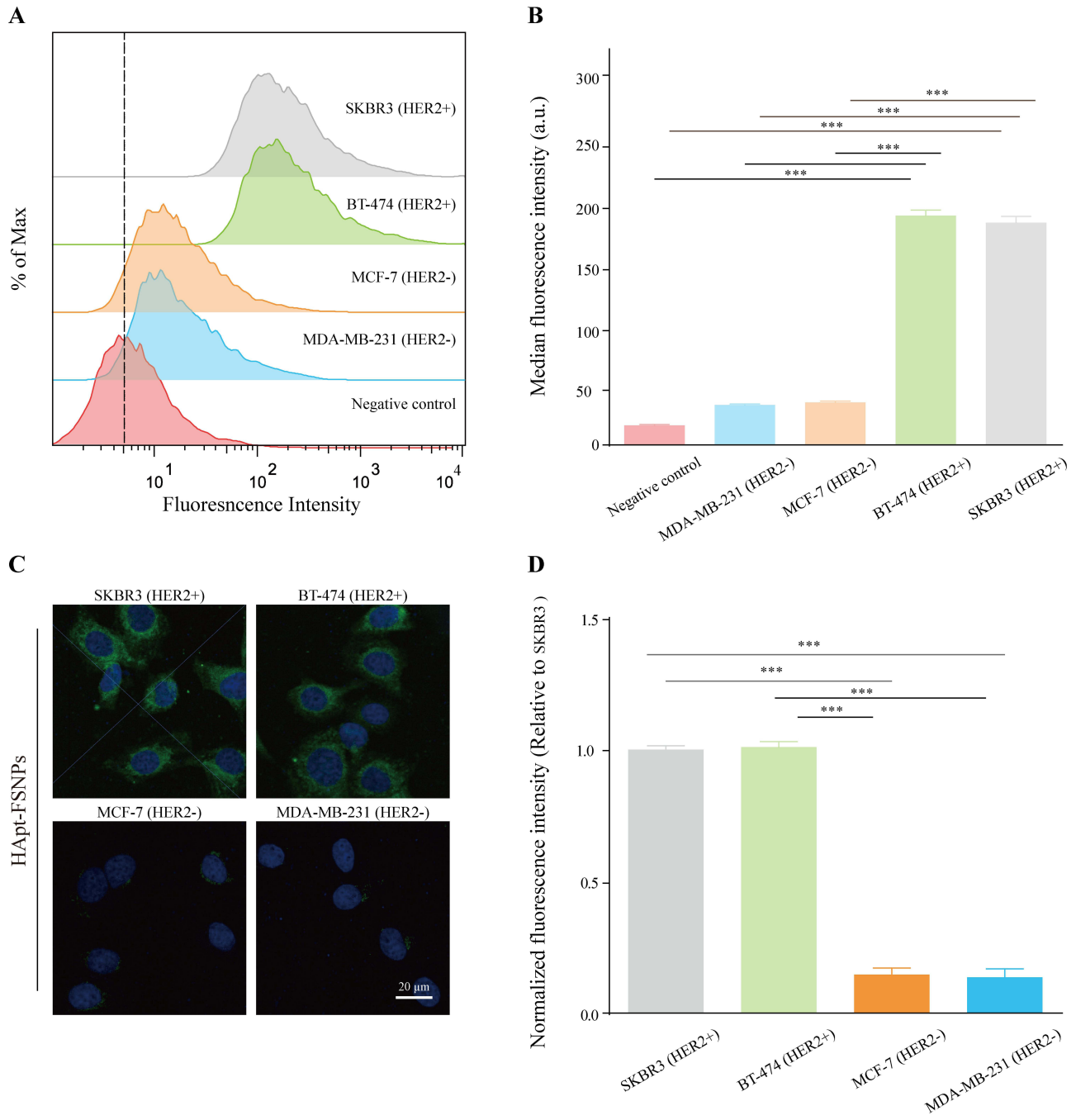

Figure 3 HApt-FSNPs enable specific recognition of HER2-positive breast cancer cells.

Tumor Tissue Section Validation of HApt-FSNPs Specificity

To further validate the specificity of HApt-FSNPs at the tissue level, HER2-positive (SKBR3) and HER2-negative (MCF-7) tumor tissue sections were treated with FSNPs, Scr-FSNPs, HApt-FSNPs, and HApt-FSNPs with competitive blocking by excess free HApt (Blocking) (Figure 5). Figure 5A shows fluorescence microscopy images of HER2-positive tumor sections, where HApt-FSNPs bind specifically to HER2-positive cells, indicated by strong green fluorescence. Figure 5B quantifies normalized fluorescence intensity, showing a significant increase in fluorescence with HApt-FSNPs ($P < 0.001$) compared to FSNPs, Scr-FSNPs, and blocking groups. Figure 5C shows HER2-negative tumor sections, where minimal fluorescence is observed in all treatment groups. Figure 5D quantifies fluorescence intensity, showing no significant difference across the groups,

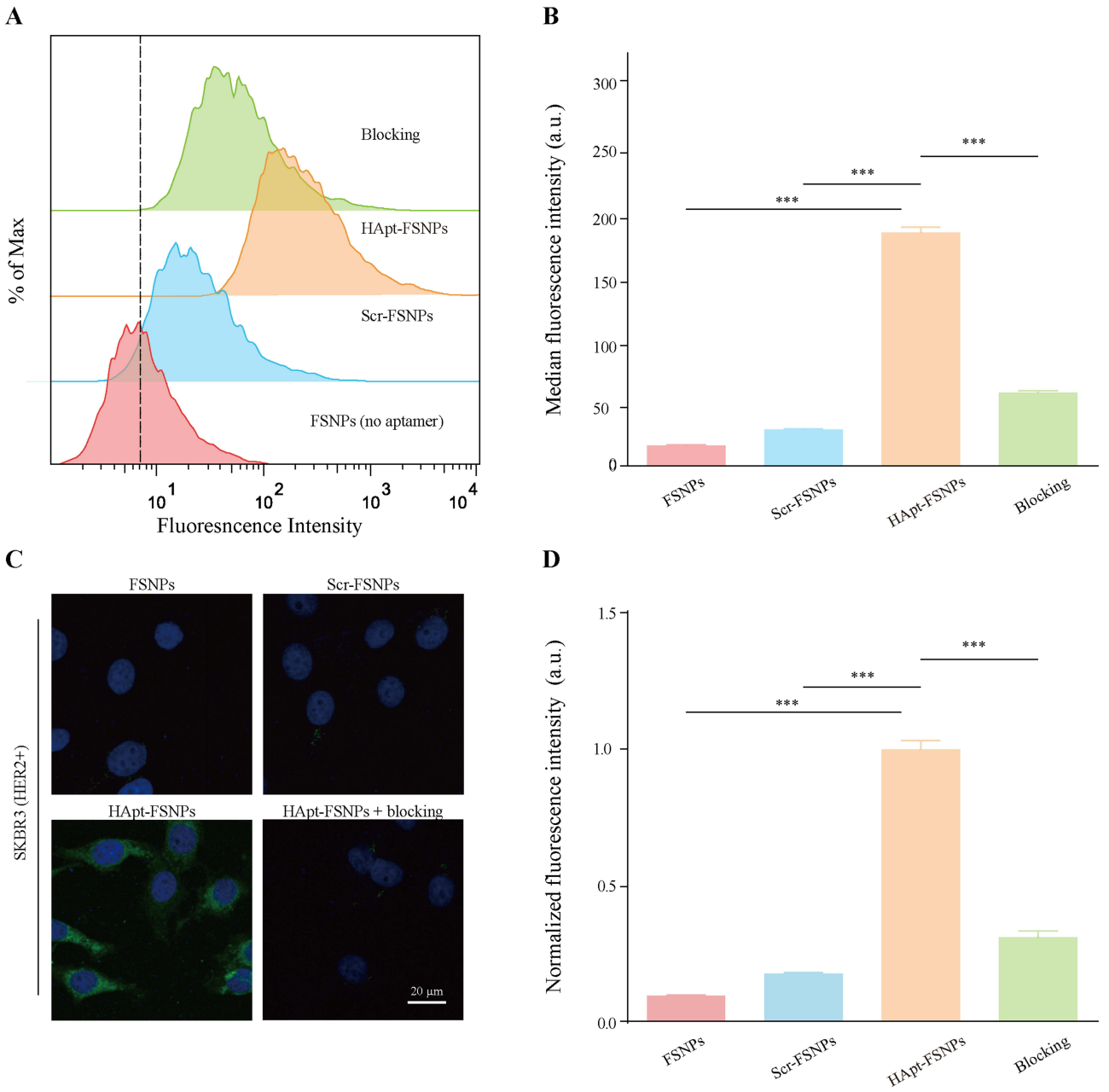

Figure 4 Specificity controls and competitive blocking of HApt-FSNP binding to HER2-positive breast cancer cells (SKBR3). (**A**) Flow-cytometry histogram overlays of fluorescence intensity after incubation with bare FSNPs (no aptamer), Scr-FSNPs, HApt-FSNPs, or HApt-FSNPs with competitive blocking by excess free HApt (Blocking). (**B**) Quantification of flow-cytometry signals shown as MFI (a.u). (**C**) Representative fluorescence microscopy images of SKBR3 cells treated with the indicated formulations (green, FSNP fluorescence; blue, nuclei). (**D**) Microscopy quantification of normalized fluorescence intensity per field (HApt-FSNP group set to 1). Data are presented as mean ± SD; ***P < 0.001.

confirming the specificity of HApt-FSNPs. These results confirm that HApt-FSNPs are capable of selectively targeting HER2-positive tumor tissue.

In vivo Fluorescence Imaging and Biodistribution of HApt-FSNPs

The in vivo targeting efficacy and biodistribution of HApt-FSNPs were evaluated in tumor-bearing mouse models. As presented in Figure 6A, whole-body fluorescence imaging at sequential time points (0.5, 2, 6, 12, and 24 h) after tail vein administration revealed clear time-dependent accumulation of nanoparticles in HER2-positive (SKBR3) tumors, with signal intensity peaking at 6 h post-injection. Quantitative analysis further demonstrated the targeting specificity of HApt-

https://doi.org/10.2147/IJN.S591943

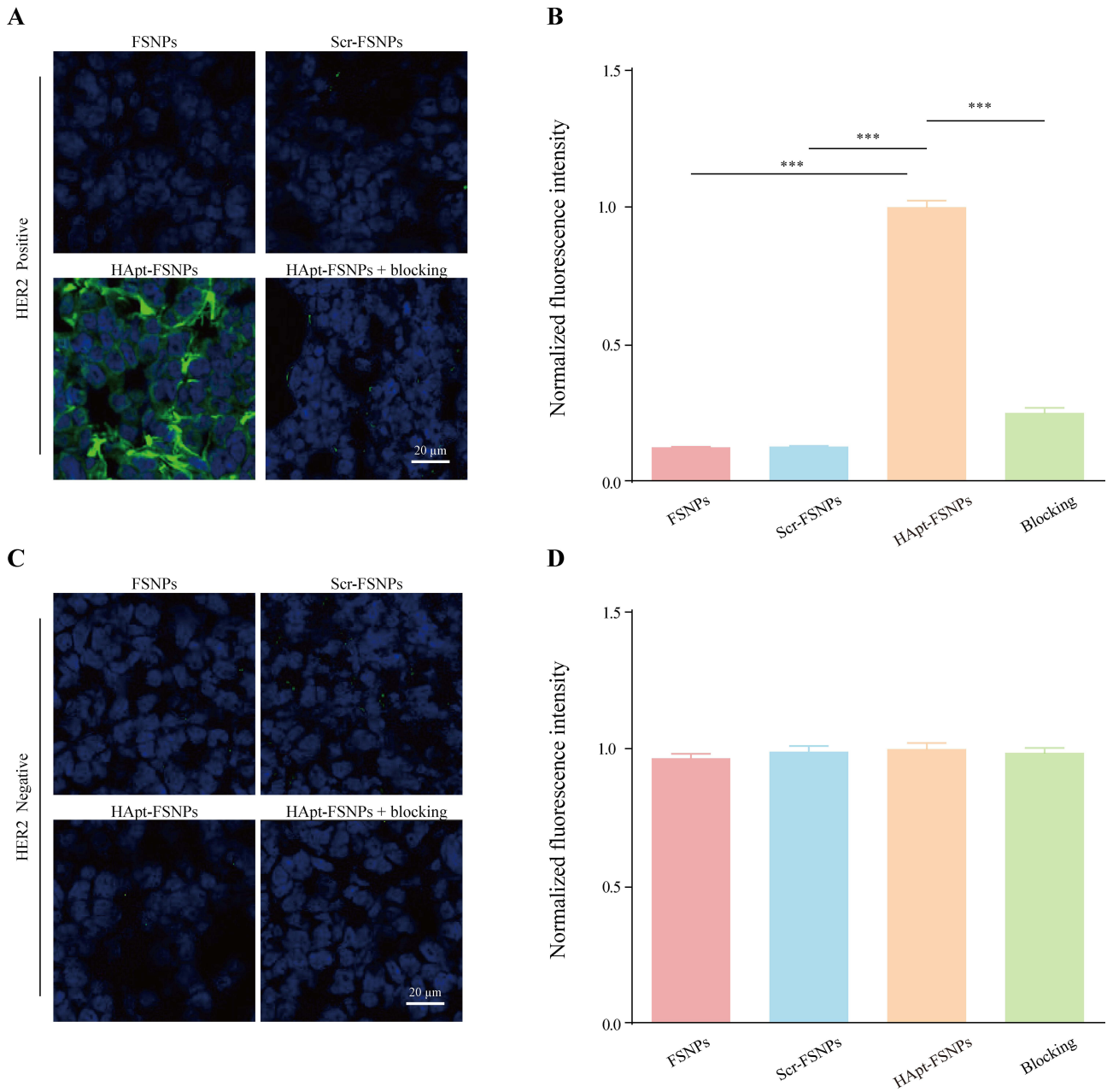

Figure 5 HApt-FSNPs for specificity validation in HER2-positive and HER2-negative tumor tissue sections. (**A**) Fluorescence microscopy of HER2-positive (SKBR3) tumor sections treated with FSNPs, Scr-FSNPs, HApt-FSNPs, or HApt-FSNPs with blocking. Green = HApt-FSNPs, blue = DAPI-stained nuclei. (**B**) Normalized fluorescence intensity of HER2-positive tumor sections, showing significant increase with HApt-FSNPs ($P < 0.001$). (**C**) Fluorescence microscopy of HER2-negative (MCF-7) tumor sections treated with the same formulations. (**D**) Normalized fluorescence intensity of HER2-negative tumor sections, showing no significant difference across groups. Data are mean ± SD; ***$P < 0.001$.

FSNPs. The fluorescence intensity in HER2-positive tumors was significantly higher than that in HER2-negative (MCF-7) tumors across all observed time points (Figure 6B), with the most pronounced difference noted at 6 h ($p < 0.001$), supporting receptor-specific delivery in vivo.

Ex vivo imaging of excised organs and tumors provided additional evidence of selective tumor targeting (Figure 6C). HApt-FSNPs exhibited preferential accumulation in HER2-positive tumors, whereas only minimal fluorescence was detected in major organs (heart, lungs, liver, kidneys, spleen) and HER2-negative tumors. Quantitative assessment of fluorescence signals in harvested tissues (Figure 6D) confirmed a marked increase in HER2-positive tumor accumulation compared to both HER2-negative tumors and normal organs, consistent with the in vivo imaging observations.

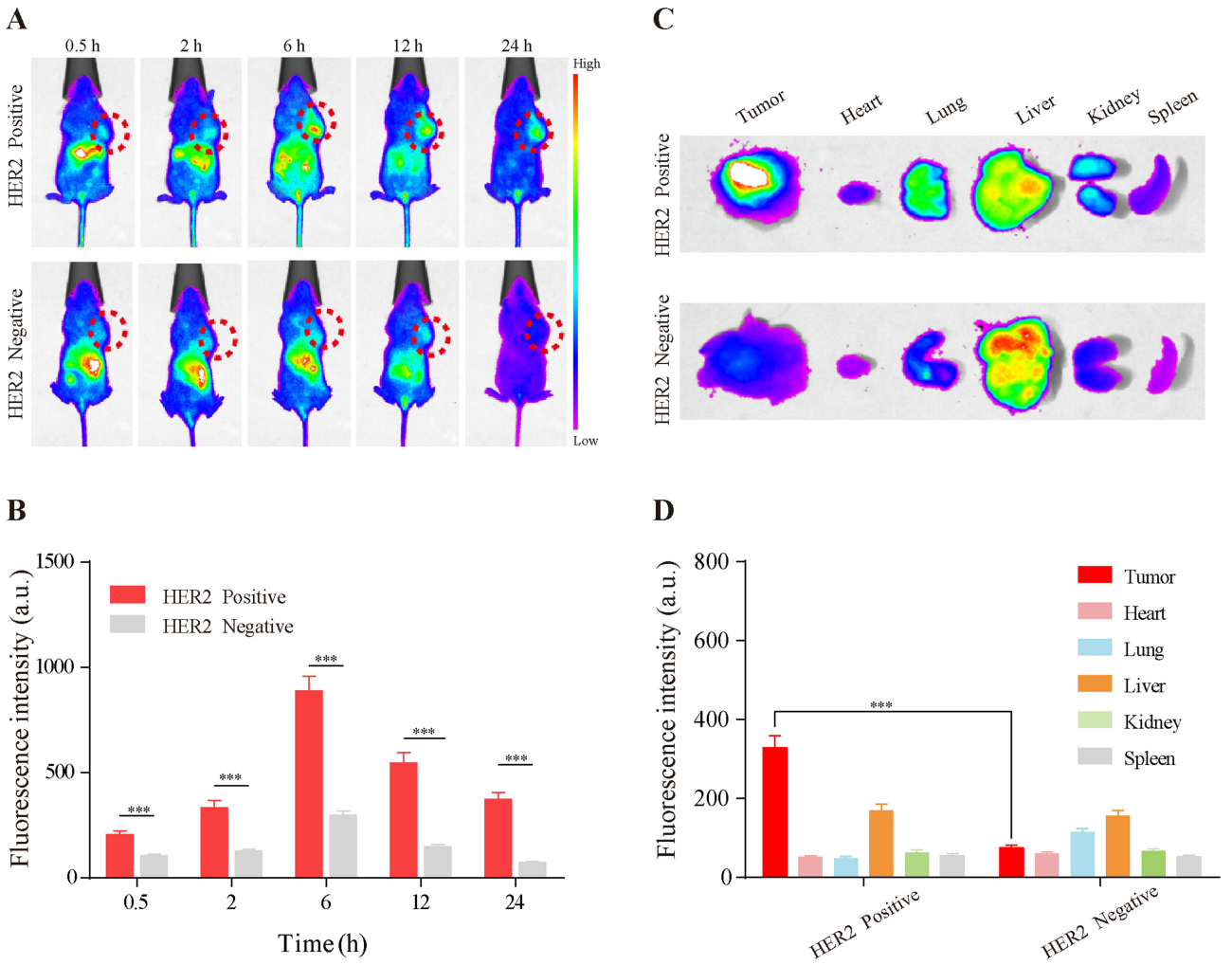

Figure 6 In Vivo Fluorescence Imaging and Biodistribution of HApt-FSNPs in Tumor-Bearing Mice. (**A**) Whole-body fluorescence images of tumor-bearing mice at various time points (0.5, 2, 6, 12, 24 hours) after tail vein injection of HApt-FSNPs. The accumulation of nanoparticles in HER2-positive tumors is indicated by increased fluorescence intensity. The tumor regions are highlighted with red dotted circles. (**B**) Quantification of fluorescence intensity in HER2-positive and HER2-negative tumor regions over time. (**C**) Ex vivo fluorescence images of major organs (heart, lungs, liver, spleen, kidney) and tumors harvested after systemic injection, showing selective accumulation in HER2-positive tumors. (**D**) Quantitativeanalysis of ex vivo fluorescence intensity in the tumor and major organs. ***p< 0.001.

Enhanced Photostability of HApt-FSNPs

The photostability of HApt-FSNPs was evaluated in comparison with free FITC-labeled HApt under continuous illumination (Figure 7). Time-lapse fluorescence imaging demonstrated that HApt-FSNPs maintained a stable fluorescence signal over time, whereas free FITC-HApt exhibited rapid photobleaching (Figure 7A). Quantitative analysis of normalized fluorescence intensity further confirmed that HApt-FSNPs retained a substantially higher proportion of their initial fluorescence signal throughout the observation period (Figure 7B), highlighting the protective effect of the silica matrix on the encapsulated fluorophores.

In vitro Cytocompatibility and in vivo Biosafety Evaluation

The biocompatibility of HApt-FSNPs was systematically assessed both in vitro and in vivo (Figure 8). CCK-8 assays showed that HApt-FSNPs exhibited negligible cytotoxicity toward HEK293T and L-02 cells across a range of concentrations (0.1–1.0 mg/mL) and incubation times (12–48 h), with cell viability consistently remaining above 90% (Figure 8A).

In vivo biosafety was evaluated by histological analysis of major organs collected seven days after administration of HApt-FSNPs. Hematoxylin and eosin (H&E) staining revealed normal tissue architecture in the heart, lung, liver, spleen,

https://doi.org/10.2147/IJN.S591943

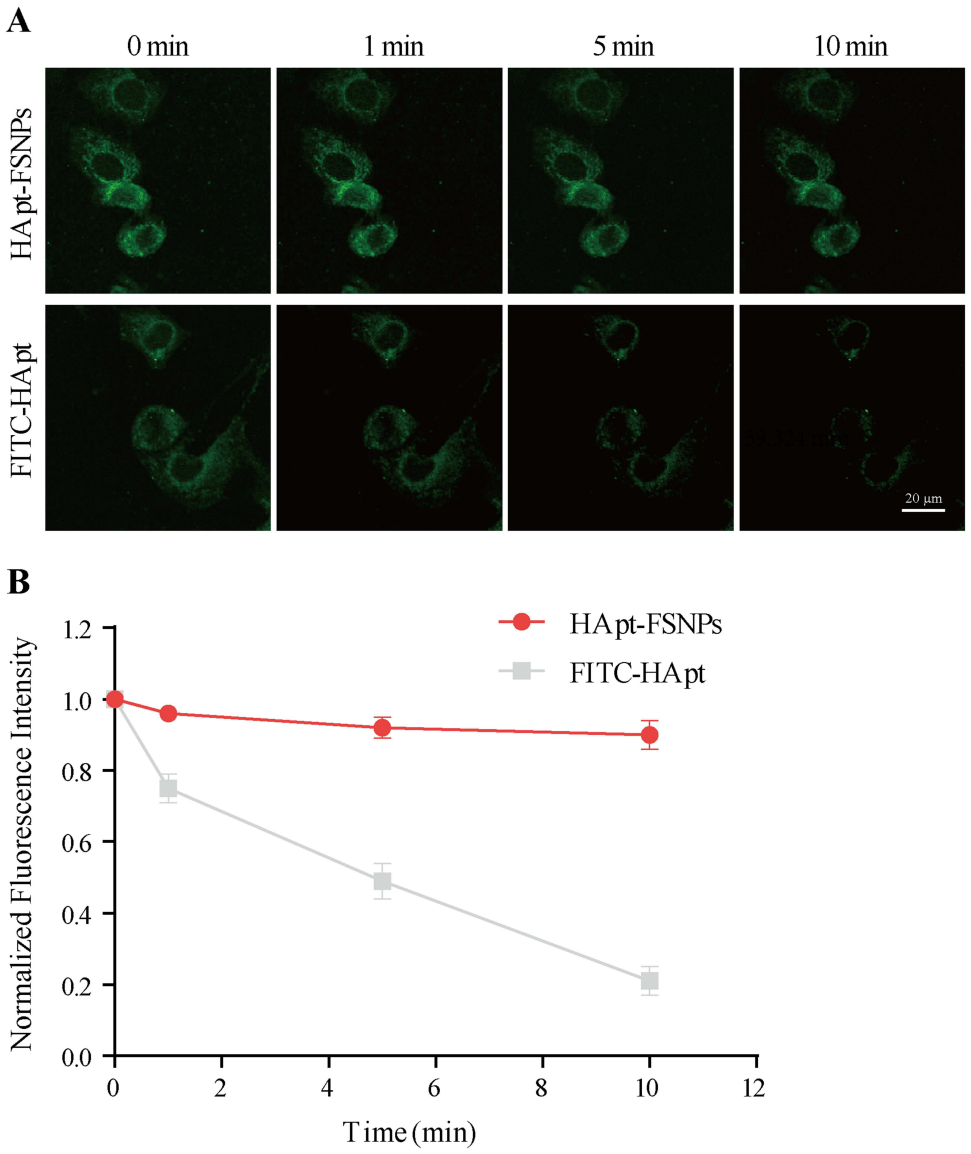

Figure 7 Photostability of HApt-FSNPs compared with free FITC-labeled HApt. (**A**) Time-lapse fluorescence microscopy images acquired at 0, 1, 5, and 10 min after continuous illumination, showing that HApt-FSNPs maintain a stable fluorescence signal whereas FITC-HApt undergoes rapid photobleaching. (**B**) Quantification of normalized fluorescence intensity over time (normalized to 0 min). Data are presented as mean ± SD from multiple fields of view.

and kidney, with no observable pathological abnormalities compared with PBS-treated controls (Figure 8B). These results indicate that HApt-FSNPs possess favorable biocompatibility and do not induce detectable organ toxicity under the tested conditions.

Discussion

In this study, we developed a HER2 aptamer–functionalized fluorescent silica nanoparticle platform for the highly specific detection of HER2-positive breast cancer cells. By integrating the molecular recognition capability of a HER2-specific DNA aptamer with the signal amplification and photostability advantages of FSNPs, the HApt-FSNP system achieved selective binding to HER2-positive cells while maintaining excellent optical stability and biosafety. These characteristics position HApt-FSNPs as a promising pre-therapeutic diagnostic tool for molecular subtyping of breast cancer. These findings highlight the potential of HApt-FSNPs as a promising platform for further development as a targeted imaging probe.

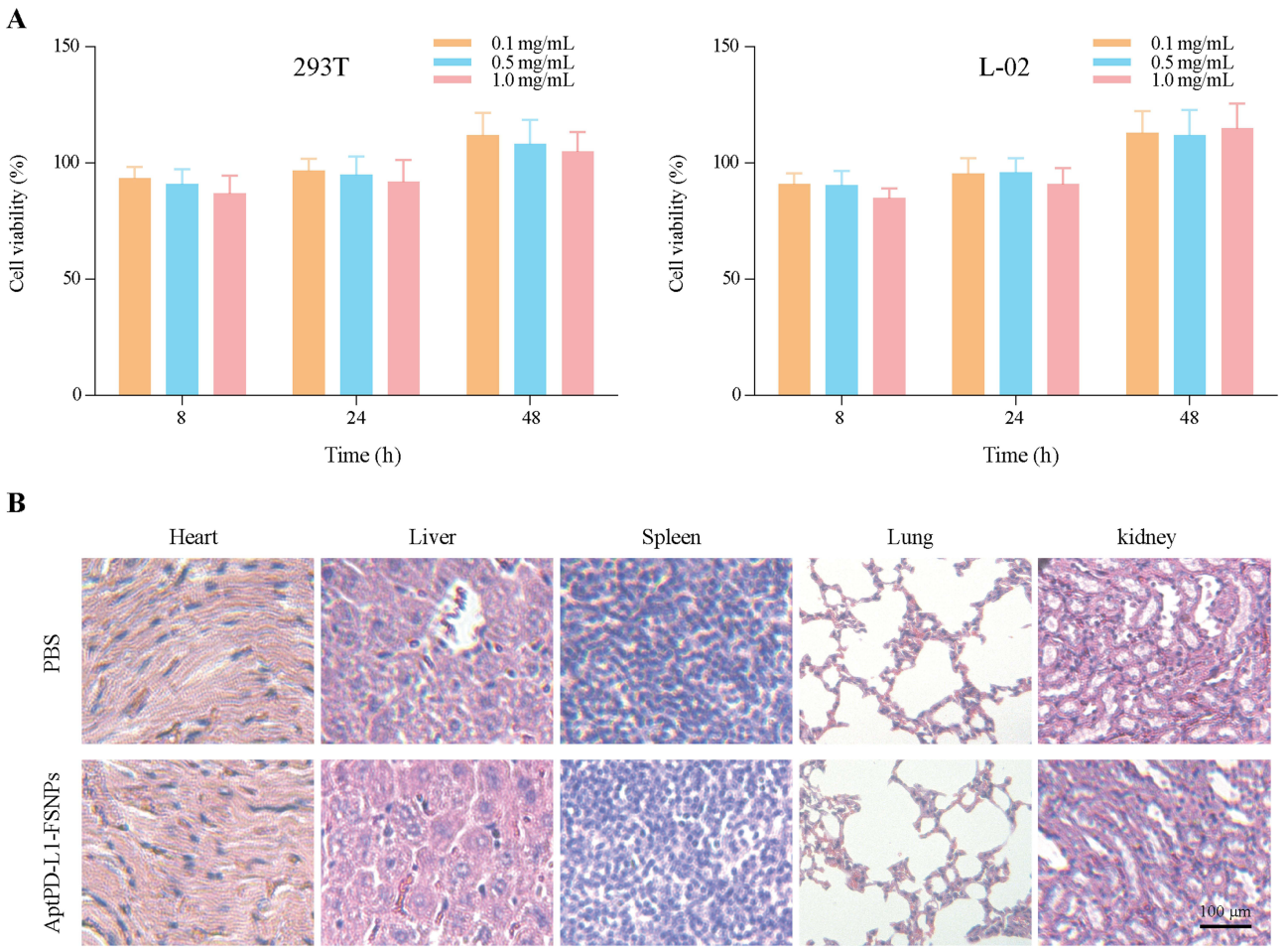

Figure 8 In vitro cytocompatibility and in vivo biosafety evaluation of HApt-FSNPs. (**A**) Cell viability of HEK293T and L-02 cells after incubation with HApt-FSNPs at 0.1, 0.5, and 1.0 mg/mL for 12, 24, and 48 h (CCK-8 assay). (**B**) Representative H&E-stained sections of major organs (heart, lung, liver, spleen, and kidney) collected from mice treated with HApt-FSNPs or PBS, showing no apparent histopathological abnormalities.

A key strength of the HApt-FSNP platform lies in its aptamer-mediated molecular recognition. Aptamers recognize targets through defined three-dimensional conformations and noncovalent interactions, providing high affinity and specificity comparable to antibodies, but without the intrinsic limitations associated with protein-based ligands.[25–27] HApt-FSNPs demonstrated strong binding to HER2-positive SKBR3 and BT-474 cells, with negligible interaction observed in HER2-negative cell lines. Competitive blocking experiments confirmed that targeting was specifically driven by HApt–HER2 interactions, ensuring minimal background signals and enhanced detection accuracy. The specificity of HApt-FSNPs was further validated at the tissue level using HER2-positive and HER2-negative tumor sections. The significant accumulation of HApt-FSNPs in HER2-positive tumors, with peak fluorescence at 6 hours post-injection, and the minimal signal in HER2-negative tumors provide compelling evidence of target-specific delivery in a living system.

Compared with conventional antibody-based fluorescent probes, HApt-FSNPs offer several notable advantages. Antibodies often suffer from batch-to-batch variability, limited chemical stability, and susceptibility to denaturation during conjugation or storage.[28] In contrast, DNA aptamers are chemically synthesized, structurally stable, and amenable to precise and reproducible surface modification.[29] Moreover, the nanoscale architecture of FSNPs allows multiple fluorescent moieties to be encapsulated within a single particle, resulting in signal amplification that is difficult to achieve with single fluorophore–antibody conjugates. The observed increase in particle size and surface charge shift after aptamer conjugation further confirmed the successful construction of a well-defined targeting nanostructure.[23]

https://doi.org/10.2147/IJN.S591943

Photostability is another critical factor for reliable fluorescence-based detection and imaging. Organic dyes and dye-labeled aptamers are prone to rapid photobleaching under continuous excitation, which limits their usefulness for prolonged observation or quantitative analysis.[30] In this study, HApt-FSNPs demonstrated markedly enhanced photostability compared with free FITC-labeled HApt, retaining strong fluorescence signals even after extended illumination. This improvement, attributed to the protective silica matrix,[31] was instrumental in enabling the clear, time-dependent visualization of tumor targeting in our in vivo imaging experiments.

Biosafety is a prerequisite for the translational application of nanomaterials.[32–34] The HApt-FSNPs exhibited minimal cytotoxicity toward normal human cell lines across a range of concentrations and incubation times, indicating good in vitro cytocompatibility. Importantly, in vivo histological analysis revealed no apparent pathological abnormalities in major organs. Furthermore, the biodistribution data from our in vivo imaging study showed that while some accumulation occurred in the liver and spleen—a common pathway for nanoparticle clearance—the fluorescence signal was predominantly and specifically localized to HER2-positive tumors, supporting a favorable safety and specificity profile for diagnostic use.

Clinically, the ability to non-invasively identify HER2 status through in vivo imaging could provide crucial insights for treatment planning. By serving as a molecular subtyping tool, this probe may help guide the selection of appropriate HER2-targeted therapies, thereby contributing to the advancement of precision medicine in breast cancer management.

From a broader perspective, the HApt-FSNP strategy represents a versatile and modular approach for cancer biomarker detection. By simply altering the aptamer sequence, this platform could be readily adapted to target other tumor-associated receptors or molecular signatures. In addition, the fluorescent silica nanoparticle core provides opportunities for further functional integration, such as multimodal imaging or theranostic applications. These features underscore the flexibility and extensibility of the proposed system.

While this study provides comprehensive validation from cells to live animals, some limitations remain for clinical translation. First, the current study focused on qualitative assessments of fluorescence intensity to demonstrate targeting specificity. To fully characterize the sensitivity and potential for clinical use, future work should address quantitative metrics such as the limit of detection, signal-to-noise ratio, and the ability to detect early-stage lesions. These factors are critical for advancing HApt-FSNPs as a reliable diagnostic tool for clinical settings. Furthermore, future work should evaluate the platform's performance in human-derived models or clinical samples to better mimic the heterogeneity of human tumors and assess its clinical diagnostic capabilities.

In summary, this study demonstrates that HApt-FSNPs enable highly specific, photostable, and biocompatible detection and imaging of HER2-positive breast cancer from the cellular level to in vivo tumor models. The successful demonstration of specific tumor accumulation via systemic delivery validates HApt-FSNPs as a promising bioimaging probe, moving this platform closer to clinical applications as a diagnostic tool for molecular subtyping and treatment guidance.

Conclusion

In conclusion, this study demonstrates that HApt-FSNPs enable specific detection and imaging of HER2-positive breast cancer across cellular, tissue, and in vivo levels, demonstrating favorable biosafety. This platform holds promise as a pre-therapeutic diagnostic tool to guide HER2-targeted therapy and advance precision breast cancer care.

Abbreviations

BSA, bovine serum albumin; CCK-8, Cell Counting Kit-8; DLS, dynamic light scattering; FITC, fluorescein isothiocyanate; FISH, fluorescence in situ hybridization; FT-IR, Fourier-transform infrared; FSNPs, fluorescent silica nanoparticles; HApt, HER2-specific DNA aptamer; H&E, hematoxylin and eosin; HER2, human epidermal growth factor receptor 2; HPLC, high-performance liquid chromatography; IHC, immunohistochemistry; MFI, median fluorescence intensity; OCT, optimal cutting temperature compound; PDI, polydispersity index; PBS, phosphate-buffered saline; SD, standard deviation; SELEX, Systematic Evolution of Ligands by Exponential Enrichment; Scr, scramble control aptamer;

Scr-FSNPs, scramble aptamer-functionalized fluorescent silica nanoparticles; TEOS, tetraethyl orthosilicate; TEM, transmission electron microscopy; UV-Vis, ultraviolet-visible.

Funding

There is no funding to report.

Disclosure

The authors report no conflicts of interest in this work.

References

1. Sitia L, Sevieri M, Signati L, et al. HER-2-targeted nanoparticles for breast cancer diagnosis and treatment. *Cancers*. 2022;14(10):2424. doi:10.3390/cancers14102424
2. Ma D, Dai L-J, Wu X-R, et al. Spatial determinants of antibody-drug conjugate SHR-A1811 efficacy in neoadjuvant treatment for HER2-positive breast cancer. *Cancer Cell*. 2025;43:1061–1075.e1067. doi:10.1016/j.ccell.2025.03.017
3. Cheng X, Cai H, Li X, et al. Reversing adenosine-mediated immunosuppression in triple-negative breast cancer by synergistic chemo-immunotherapy via stimuli-responsive nanomedicines. *EBioMedicine*. 2026;123:106059. doi:10.1016/j.ebiom.2025.106059
4. Su X, Liu X, Xie Y, et al. Integrated SERS-vertical flow biosensor enabling multiplexed quantitative profiling of serological exosomal proteins in patients for accurate breast cancer subtyping. *ACS Nano*. 2023;17(4):4077–4088. doi:10.1021/acsnano.3c00449
5. Roy M, Fowler AM, Ulaner GA, Mahajan A. Molecular classification of breast cancer. *PET Clin*. 2023;18:441–458. doi:10.1016/j.cpet.2023.04.002
6. Macaulay DO, Han W, Zarella MD, Garcia CA, Tavolara TE. Enhancing HER2 testing in breast cancer: predicting fluorescence in situ hybridization (FISH) scores from immunohistochemistry images via deep learning. *J Pathol Clin Res*. 2025;11:e70024. doi:10.1002/2056-4538.70024
7. Tan J, Yang N, Zhong L, et al. A new theranostic system based on endoglin aptamer conjugated fluorescent silica nanoparticles. *Theranostics*. 2017;7(19):4862–4876. doi:10.7150/thno.19101
8. Dai J, Ashrafizadeh M, Aref AR, Sethi G, Ertas YN. Peptide-functionalized, -assembled and -loaded nanoparticles in cancer therapy. *Drug Discov Today*. 2024;29:103981. doi:10.1016/j.drudis.2024.103981
9. Tan J, Zhu D, Li G, et al. A novel theranostic system of PD-L1-Aptamer-functionalized fluorescent silica nanoparticles for triple-negative breast cancer. *Nanomedicine*. 2025;68:102834. doi:10.1016/j.nano.2025.102834
10. Wang B, Hu S, Teng Y, et al. Current advance of nanotechnology in diagnosis and treatment for malignant tumors. *Signal Transduct Target Ther*. 2024;9:200. doi:10.1038/s41392-024-01889-y
11. Nasrollahpour H, Khalilzadeh B, Hasanzadeh M, et al. Nanotechnology-based electrochemical biosensors for monitoring breast cancer biomarkers. *Med Res Rev*. 2023;43(3):464–569. doi:10.1002/med.21931
12. Zhang Y, Fang Z, Pan D, et al. Dendritic polymer-based nanomedicines remodel the tumor stroma: improve drug penetration and enhance antitumor immune response. *Adv Mater*. 2024;36(25):e2401304. doi:10.1002/adma.202401304
13. Li Y, Zamay TN, Luzan NA, et al. Aptamers as a new frontier in targeted cancer therapy. *Adv Drug Deliv Rev*. 2025;226:115692. doi:10.1016/j.addr.2025.115692
14. Rawat R, Roy S, Goswami T, et al. Aptamer-enhanced ultrasensitive electrochemical detection of HER-2 in breast cancer diagnosis using ZnO tetrapod-K(4)PTC nanohybrids. *Sci Rep*. 2025;15:17173. doi:10.1038/s41598-025-88335-3
15. Mohammadinejad A, Gaman LE, Aleyaghoob G, et al. Aptamer-based targeting of cancer: a powerful tool for diagnostic and therapeutic aims. *Biosensors*. 2024;14. doi:10.3390/bios14020078
16. Feng L, Sun Y, Jia W, et al. Advancements in SELEX technology for aptamers and emerging applications in therapeutics and drug delivery. *Biomolecules*. 2025;15(6):818. doi:10.3390/biom15060818
17. Wang L, Canoura J, Byrd C, et al. Examining the relationship between aptamer complexity and molecular discrimination of a low-epitope target. *ACS Cent Sci*. 2024;10(12):2213–2228. doi:10.1021/acscentsci.4c01377
18. Iraniparast M, Kumar N, Sokolov I. Single ultrabright fluorescent silica nanoparticles can be used as individual fast real-time nanothermometers. *Mater Horiz*. 2025;12:4759–4770. doi:10.1039/d4mh01907e
19. Erstling JA, Bag N, Gardinier TC, et al. Overcoming barriers associated with oral delivery of differently sized fluorescent core-shell silica nanoparticles. *Adv Mater*. 2024;36(1):e2305937. doi:10.1002/adma.202305937
20. Tan J, Yang N, Hu Z, et al. Aptamer-functionalized fluorescent silica nanoparticles for highly sensitive detection of leukemia cells. *Nanoscale Res Lett*. 2016;11(1):298. doi:10.1186/s11671-016-1512-8
21. Islam MF, Elbayomi S, Abdulkadir A, et al. Modified Rhodamine B immobilized on silica nanoparticles (MRB@SiNPs) as a fluorescent probe for selective metal ion detection. *Luminescence*. 2025;40(6):e70216. doi:10.1002/bio.70216
22. Jo H, Her J, Ban C. Dual aptamer-functionalized silica nanoparticles for the highly sensitive detection of breast cancer. *Biosens Bioelectron*. 2015;71:129–136. doi:10.1016/j.bios.2015.04.030
23. Nakahara Y, Nakajima Y, Okada S, Miyazaki J, Yajima S. Synthesis of silica nanoparticles with physical encapsulation of near-infrared fluorescent dyes and their tannic acid coating. *ACS Omega*. 2021;6:17651–17659. doi:10.1021/acsomega.1c02204
24. *National Research Council Committee for the Update of the Guide for the, C. & Use of Laboratory, A. in Guide for the Care and Use of Laboratory Animals*. National Academies Press (US) Copyright © 2011, National Academy of Sciences, 2011).
25. Küçükcankurt F, Uçak S, Altiok N. Theranostic potential of a novel aptamer specifically targeting HER2 in breast cancer cells. *Turk J Biol*. 2024;48:35–45. doi:10.55730/1300-0152.2680
26. Liu M, Wang L, Lo Y, et al. Aptamer-enabled nanomaterials for therapeutics, drug targeting and imaging. *Cells*. 2022;11. doi:10.3390/cells11010159

27. Guan B, Zhang X. Aptamers as versatile ligands for biomedical and pharmaceutical applications. *Int J Nanomed*. 2020;15:1059–1071. doi:10.2147/ijn.S237544
28. Agnello L, Camorani S, Fedele M, Cerchia L. Aptamers and antibodies: rivals or allies in cancer targeted therapy? *Explor Target Antitumor Ther*. 2021;2:107–121. doi:10.37349/etat.2021.00035
29. Domsicova M, Korcekova J, Poturnayova A, Breier A. New insights into aptamers: an alternative to antibodies in the detection of molecular biomarkers. *Int J Mol Sci*. 2024;25(13):6833. doi:10.3390/ijms25136833
30. Hei Y, Wang B, He Y, et al. Photostability of organic fluorophore influenced by adjacent amino acid residues. *Commun Chem*. 2025;8(1):262. doi:10.1038/s42004-025-01661-5
31. Stenspil SG, Laursen BW. Photophysics of fluorescent nanoparticles based on organic dyes - challenges and design principles. *Chem Sci*. 2024;15:8625–8638. doi:10.1039/d4sc01352b
32. Janjua TI, Cao Y, Kleitz F, et al. Silica nanoparticles: a review of their safety and current strategies to overcome biological barriers. *Adv Drug Deliv Rev*. 2023;203:115115. doi:10.1016/j.addr.2023.115115
33. Lérida-Viso A, Estepa-Fernández A, García-Fernández A, Martí-Centelles V, Martínez-Máñez R. Biosafety of mesoporous silica nanoparticles; towards clinical translation. *Adv Drug Deliv Rev*. 2023;201:115049. doi:10.1016/j.addr.2023.115049
34. Shen X, Cai H, Wang Y, et al. Metabolic targeting of oxidative phosphorylation enhances chemosensitivity in triple-negative breast cancer via a synergistic nanomedicine. *Theranostics*. 2025;15(15):7607–7626. doi:10.7150/thno.116250